Induction Heating System for Industrial Bearings or Common Appliances

3

Alexandre Diogo Leites da Silva,
José Alberto Campos Neves, and Nelson Neves

3.1 Introduction

The conventional methods for heating steel bearings, to facilitate their placement on a machine shaft, such as engines and alternators, are open flame, oil bath heating, resistive plates and resistive furnace heaters.

According to SKF (2022), the first solution brings risks to the user and can cause structural damage to the bearing. The second solution is environmentally unadvisable, besides contaminating the bearing with oil and possibly compromising its future performance. The third solution is characterized by excessive thermal energy loss. The fourth solution, although more efficient than the previous one, is more expensive, due to the cost of the furnace. In addition, the clogging of the furnace to accommodate large bearings makes it difficult to heat them near the electric machine shaft, increasing risks of improper bearing assembly.

Currently, induction heating is one of the key metal industry applications, based on three main effects: electromagnetic induction, skin effect and heat transfer. The proposed system uses an electronic power converter for coil current control, and consequently, the temperature, an AVR microcontroller plus a set of sensors to measure the necessary variables of the induction heating process. Such system reduces the risk of incorrect use and improves energy efficiency (Mohan et al., 2003) when compared to conventional heating devices. This work aims to develop high-energy efficiency induction heater system, without environmental risks, that minimizes

A. D. L. da Silva (✉) · N. Neves
ISPGAYA, Vila Nova de Gaia, Portugal
e-mail: adiogo@ispgaya.pt

J. A. C. Neves
ISPGAYA, Vila Nova de Gaia, Portugal

ISVOUGA, Santa Maria da Feira, Portugal

F. L. Almeida et al. (eds.), *Multidimensional Sustainability: Transitions and Convergences*, Springer Proceedings in Earth and Environmental Sciences,
https://doi.org/10.1007/978-3-031-24892-4_3

problems of inadequate assembly, and fulfilling the requirements of the heating process of steel alloys bearings. This induction-based heater guarantees the appropriate process temperature as the temperature differential between the inner and outer rings, within manufacturer specified limits.

This chapter is divided into five parts. In the first part, presents an introduction to the subject. The second part is a review of the induction heating methods. The third part describes the applied method, and in the fourth, results are presented and evaluated. Finally, a conclusion is drawn up indicating practical implications, limitations and other issues as well as future lines of development.

3.2 Literature Review

In induction heating, the temperature rise in the workpiece is caused by its electrical conduction characteristic. This phenomenon is called Foucault currents, also known as Eddy currents, caused by electromagnetic induction (Umans et al., 2014) that is frequency dependent. When compared to conventional heating systems, as is the case of oil bath heating, open flame heating and resistive furnace heaters, induction heating is safe, clean, quick and efficient (Mohan et al., 2003), allowing a defined section of the workpiece to be heated accurately. This is the heating technology of choice in many industrial, domestic (Khatroth et al., 2021) and medical applications due to its advantages regarding efficiency (Lucia et al., 2013), heating speed, safety, cleanness and accurate control. Low frequency and high frequency power converters are, both, used in induction heaters (Mohan et al., 2003; Shen et al., 2006).

The magnitude of the induced currents in workpiece decreases exponentially with the distance x from the surface, by the equation $I_{(x)} = I_0 e^{-x/\delta}$ where I_0 is the current at the surface and and δ is the penetration depth at which the current is reduced to I_0 times a factor $1/e$ (Mohan et al., 2003). The penetration depth is inversely proportional to the square root of the frequency f (Hz) and the magnetic permeability μ (H/m) of the workpiece and is proportional to the square root of the material resistivity ρ (Ω.m), as shown by Eq. 3.1 (Mohan et al., 2003; Rudnev et al., 2017).

$$\delta = \sqrt{\frac{\rho}{\pi . f . \mu_r \mu_0}} \tag{3.1}$$

Consequently, the workpiece apparent cross section in alternated current (S_{ac}) is smaller than the real cross section in direct current (S_{real}). The resulting effect is greater electric resistance $R_{ac} = R_{dc} \frac{S_{real}}{S_{ac}}$ that heats more by Joule effect. Figure 3.1 depicts the apparent cross section of a circular conductor carrying an alternating current.

Circulating currents are caused in the workpiece by currents in the induction coil. The induction load can be represented by an equivalent resistance R in series with the coil reactance $j\omega L$. The equivalent resistance R_{ac} is the electric resistance of the workpiece (Mohan et al., 2003), which is dependent of the penetration depth and temperature.

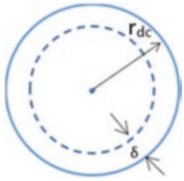

Fig. 3.1 Apparent and real cross section

Using a power converter, such an AC/AC working at constant frequency (Séguier et al., 2015), the knowledge of the current and voltage phase difference in the circuit, is essential to find the minimum value of the power switches firing angle, e.g. thyristors. In an RL load, the phase difference between voltage and current is $\varphi = \text{arctg}\left(\frac{\omega L}{R}\right)$.

The firing angle of the power switches Ψ must have the following conditions: $\varphi < \Psi < \pi$ for one thyristor and $\pi + \varphi < \pi + \Psi < 2\pi$ for the other one. Eddy currents generate, by Joule effect, a thermal power per mass unit (W/Kg), calculated by the equation: $P_e = K_e.B_{\max}^n.f^2$ (Umans et al., 2014). In this equation, B represents the density of the magnetic flux. Using a coil to produce the desired magnetic flux, its density can be calculated by applying the Ampère's Law to a solenoid (Villate, 1999) $B = \mu\frac{N}{l}I$ where I is the current in the solenoid. Thus, the thermal power developed in the workpiece and consequently its temperature depend on the control of that current.

The temperature in the workpiece can be calculated as follows (Perrot, 2010):

$$T = \left(\frac{P}{hA} + T_0\right) - \frac{P}{hA}e^{-\left(\frac{hA}{mC_p}t\right)} \tag{3.2}$$

where h is the heat transfer coefficient of air (W/m^{2}K), A is the dissipation area, m is the workpiece mass, C_p is its specific heat,T_0 is the room temperature and P is the electric power supplied. For time t long enough, the temperature T tends to the steady state value: $T = \left(\frac{P}{hA} + T_0\right)$.

The electric power needed to raise temperature to a desired value after a specified time, its calculated rearranging Eq. 3.2:

$$P = \frac{hA\left(T - T_0\right)}{\left(1 - e^{-\frac{hA}{mCp}t}\right)} \tag{3.3}$$

3.3 Methodology

The proposed solution consists in taking advantage of the temperature rise that occurs in materials, such as steel, which is caused by hysteresis losses and induced Eddy currents (Umans et al., 2014), when the workpiece is exposed to a

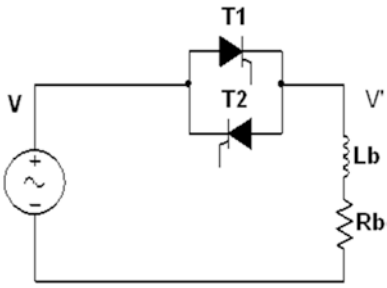

Fig. 3.2 AC/AC power converter

time-varying magnetic field. The thermal power by mass unit (W/Kg) caused by hysteresis losses is proportional to the hysteretic cycle area and is calculated by Steinmetz's empirical formula: $P_h = K_h.B_{\max}^n.f$. Eddy current losses, on the other hand, occur by Joule effect and result from the induced current in the ferromagnetic material. The thermal power by mass unit (W/Kg) caused by Eddy currents is calculated from: $P_e = K_e.B_{\max}^n.f^2$. Thus, the thermal power, by mass unit, that will raise the temperature of the workpiece is $P_t = P_h + P_e$, increasing with the amplitude of the magnetic field.

By controlling the magnitude of the magnetic induction field B, using current control in an induction coil is controlled the thermal power developed and thus the temperature. In order to keep the temperature under specific control in the heating phase, a single-phase AC/AC power electronic converter at constant frequency is used, with a microprocessor control circuit, with a feedback loop. This feedback loop of the control system uses a current sensor and an electric voltage sensor, to get the phase angle between voltage and current, along with two more sensors to measure temperatures in the bearing's inner and outer rings. Figure 3.2 shows the power converter, excluding the thyristor drive circuits, which are electrically isolated by HF transformers. In the scheme, L_b and R_b represent the inductance and ohmic resistance of the coil, respectively.

3.3.1 Calculating the Ohmic Resistance of the Induction Coil

Due to the dimensions of the ferromagnetic core of the prototype under study, the coil is limited to a maximum length l = 35 cm. Using copper conductor wire of 25 mm^2 cross section (r = 2.82 mm), coiled onto the core of straight section $A = l_1 * l_1 = 5$ cm * 5 cm, with a pitch between turns p = 7 mm, the calculated number of turns is

$$N = \frac{l}{p} = \frac{0.35}{0.007} = 50\,\text{turns}.$$

The length of the copper conductor wire obtained is

$L_{\text{cond}} = N * 4 * l_1 = 10$ m. Its ohmic resistance is, according to the physics:

$$R_b = \rho \frac{L_{\text{cond}}}{S} \tag{3.4}$$

Using Eq. 3.4, the resistivity defined for hard copper, $\rho = 0.0179\ \Omega mm^2/m$:

$$R_b = 0.0179 * \frac{10}{\pi(2.82)^2} = 7.16\,m\Omega$$

3.3.2 Calculating the Inductance of the Induction Coil, by Approximation to a Solenoid

Figure 3.3 schematically represents a solenoid. The magnetic flux density inside a solenoid of length l, with N coils ($n = N/l$ coils per meter), crossed by an electric current I_c, is obtained, by application of Ampère's Law (Villate, 1999):

$$\oint_c \vec{B}.d\vec{l} = B\int_b^a dh = B.h = \mu_0 I_{int} \Leftrightarrow Bh = \mu_0.h.\frac{N}{l}.I_c \Leftrightarrow B = \mu_0 \frac{N}{l} I_c \qquad \text{where} \qquad \mu_0$$

represents the magnetic permeability of an air core ($\mu_0 = 4\pi.10^{-7}$ H/m).

The magnetic flux through each coil is $\phi = B.A = \mu_0 \frac{N}{l} i.A$, where A is the straight section of the solenoid. From the general expression for the inductance of a coil $L = N\frac{\phi}{i}$, the inductance is

$$L = \mu_0 \frac{N^2}{l} A \tag{3.5}$$

For a core made of packed silicon steel sheets of magnetic permeability $\mu_r = 1000$, the inductance calculated with Eq. 3.5 is

$$L = \mu_r \mu_0 \frac{N^2}{l} A = 1000 * 4\pi * 10^{-7} * \frac{50^2}{0.35} * 0.05 * 0.05 = 22.4\,mH$$

The induction coil will, therefore, have an impedance:

$$Z = \sqrt{R^2 + X^2} = 7\arg(-90°)\,\Omega, \text{for } f = 50\,Hz.$$

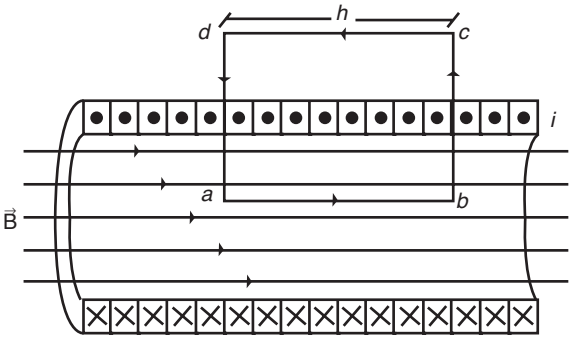

Fig. 3.3 Representation of a solenoid. (Source: Villate, 1999)

So, under a voltage of 230 V_{rms}, it would have a current intensity $I_c = 33$ A (7.5 KVA). Therefore, thyristors in the converter will need to have a stipulated current $I_{rms} > \frac{33}{\sqrt{2}} = 23\text{A}$.

3.3.3 AC/AC Converter with RL Load

Knowing the phase difference between the current and voltage in the circuit is essential to calculate the minimum value of the thyristor firing angle (Séguier et al., 2015). In *RL* loads, there is a phase difference between the voltage and current $\varphi = \text{arctg}\left(\frac{\omega L}{R}\right)$. The firing angle of the thyristors Ψ must have the following conditions: $\varphi < \Psi < \pi$ for the thyristor T_1 and $\pi + \varphi < \pi + \Psi < 2\pi$ for thyristor T_2. Firing one of the thyristors, for instance T_1 with $\Psi < \varphi$, leads to one of the undesirable operating scenarios depending on the type of command signal. Using a pulse at the thyristor gate, it is obtained a rectified current in half-wave, so the coil would be crossed by direct current of very high value, limited only by the ohmic resistances of the coil and the conductors connecting to the electrical installation. In case of using a pulse train of width $\pi - \Psi$ radians, the current will be sinusoidal with an effective value limited to $I = V/Z$, but without the possibility of control. As will be shown later, this mode of operation is used at system *start-up* and during two cycles of the grid voltage, to calculate, at runtime, the initial phase angle of the load circuit. In some circumstances, it is possible to run the heater at full power with sinusoidal current.

Figure 3.4 depicts the current and voltage waveforms in the induction coil using a suitable thyristor firing angle. It should also be noted that the control range of the converter will be $(\pi - \phi)$ radians. However, this is not a real scenario, because, as already mentioned, the coil inductance is in series with the workpiece electric resistance, which is directly proportional to the temperature and inversely proportional to the penetration depth of the Eddy currents. This means that the control range of the power converter is a little greater than 90°.

3.3.4 Command Characteristic with RL Load

The end-of-conduction angle θ_1 of a thyristor can be calculated as follows:

$$\sin(\theta_1 - \varphi) = \sin(\Psi - \varphi)e^{-\frac{\theta_1 - \Psi}{Q}} \text{ where } Q = \frac{\omega L}{R}.$$

Note that for a purely resistive load, we get $\theta_1 = \pi$ radians.

The effective value of the voltage at the load comes: $V' = V.\sqrt{\frac{\theta_1 - \Psi}{\pi} - \frac{1}{2}.\frac{\sin 2\theta_1 - \sin 2\Psi}{\pi}}$

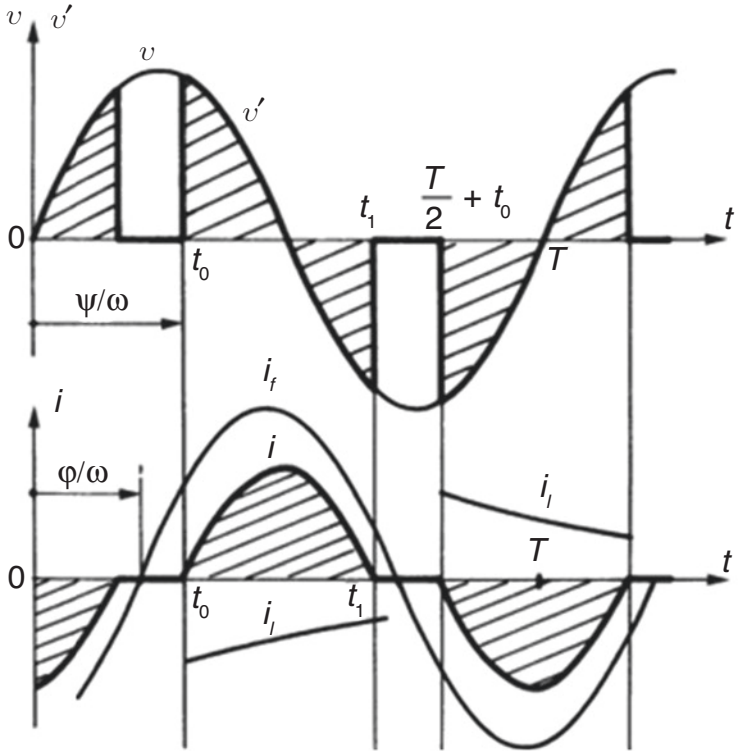

Fig. 3.4 Load voltage and current. (Source: Séguier et al., 2015)

whose Fourier series development leads to V_1', V_3', V_5', V'_7, etc. The effective value of the first harmonics of the current in the coil can obtained by

$$I_1 = \frac{V_1^{'}}{\sqrt{R^2 + (\omega L)^2}} = \frac{V_1^{'}}{R\sqrt{1+Q^2}}, I_3 = \frac{V_3^{'}}{R\sqrt{1+9Q^2}},$$

$$I_5 = \frac{V_5^{'}}{R\sqrt{1+25Q^2}}$$

For predominantly inductive loads, i.e. with $\varphi > 45°$, as is the case of our load, the effective value of the 3rd harmonic is higher than the effective value of the fundamental component of the current, for very high firing angles, i.e. for a low power operation scenario (Séguier et al., 2015).

As already explained, the thermal power generated by mass unit in the workpiece – due to hysteresis and Eddy currents – increases with the density of the magnetic flux in the coil $\left(B = \mu_0 \mu_r \frac{N}{l} I_c \right)$, which in turn is directly proportional to the

current. Thus, the power adjustment can be done by adjusting the firing angle Ψ of the thyristors, in the range $\varphi < \Psi < \pi$ for thyristor T_1 and $\pi + \varphi < \pi + \Psi < 2\pi$ for thyristor T_2.

3.3.5 System Architecture

Figure 3.5 shows the circuit diagram of the induction heating system, and Fig. 3.6 schematically represents its physical structure.

The core of the control system is an ATmega328p microcontroller (Microchip, 2022) with some features that should be highlighted:

- Analog to digital converter with 10 bits of resolution and acquisition rate up to 10,000 samples per second
- Eight-channel analog multiplexer
- Fourteen I/O ports, two of which offer interrupt facility to the CPU
- 32 Kb of Flash memory, 1 Kb of EEPROM and 2 Kb of SRAM and RS232, I²C and SPI communication facilities

Two of the analogic inputs, A_0 and A_1, are required to acquire the current in the induction coil and the grid voltage using the G_1 trans-resistance amplifier and the G_2 precision active rectifier, respectively.

Two digital I/O ports, Int_1 and Int_2, which provide interrupting facilities, are connected to the zero crossing detection circuits (ZCC) of the voltage and current signals, enabling the run-time measurement of the phase angle φ between grid voltage and current in the induction coil. In addition, the ZCC associated with the grid voltage makes it possible to find, in runtime, the delay to be generated for the firing angle of the power converter thyristors.

Temperature measurement sensors on the inner and outer bearing rings, T_{C1} and T_{C2}, respectively, connect to other analogic inputs A_2 and A_3 of the microcontroller,

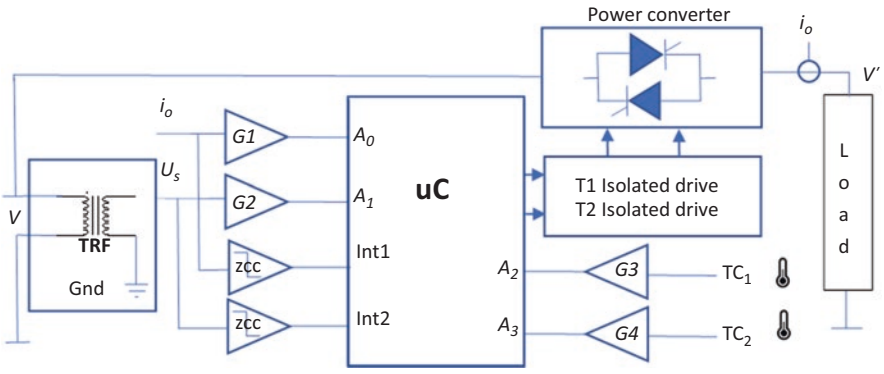

Fig. 3.5 Circuit diagram

through the cold junction temperature-compensated voltage amplifiers, G_3 and G_4. The operator's interface is user friendly, using an alphanumeric LCD display with I^2C interface and a small keyboard.

3.3.6 Thermal Behaviour

Figure 3.6 depicts the physical structure of the induction heater.

Assuming that there are no losses, the energy required to raise the temperature from T_0 to T of a workpiece of mass m and specific heat C_p is $W = m.\ C_p.\ (T - T_0)$.

And the needed power is

$$P = m.C_p \frac{dT}{dt}. \tag{3.6}$$

Therefore, the temperature increases linearly with time: $T = T_0 + \frac{P}{m.C_p} t$

However, because there are convection and conduction losses:

$$P_{\text{loss}} = hA\left(T - T_0\right) \tag{3.7}$$

Equation 3.6 must be written to:

$$P - P_{\text{loss}} = m.C_p \frac{dT}{dt}$$

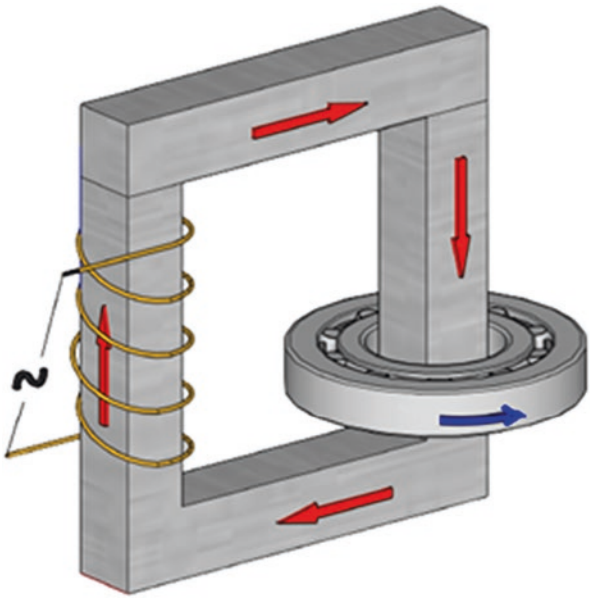

Fig. 3.6 Physical structure

Solving this differential equation, it is obtained the equation to calculate the temperature of the workpiece (Perrot, 2010):

$$T = T_0 + \frac{P}{hA}\left(1 - e^{-\frac{hA}{mC_p}t}\right) \tag{3.8}$$

In Eq. 3.8, h is the air heat transfer coefficient (W/m^{2}K), A is the workpiece thermal contact area, T is its temperature and T_0 is the room temperature. For the workpiece with the shape depicted in Fig. 3.7, the thermal contact area is

$$A = 2A_1 + A_2$$

where:

$$A_1 = \pi\left[\left(D/2\right)^2 - \left(d/2\right)^2\right]$$

and:

$$A_2 = \pi Db$$

It is shown by Eq. 3.8 that in steady state, the workpiece temperature will be: $T = T_0 + \frac{P}{hA}$

There is a wide range of bearings, with great variety in characteristics such as mass and diameter, from 0,009 kg–5 mm to 1200 kg–800 mm. Taking as reference SKF's recommendation (SKF, 2022) and the good practices of electric machine manufacturers – e.g. Asea Brown Boveri (Radvan, 2014), the temperature in the bearings should be raised from 20 to 110 °C in approximately 20 min, before they are placed on the shaft of the electric machine. Figure 3.8 shows the temperature evolution, calculated using Eq. 3.8, when providing the power equal to the workpiece's convection and conduction losses – as defined in Eq. 3.7 – to heat a workpiece with the following characteristics: D = 140 mm, d = 80 mm, b = 26 mm; m = 1650 g. For steel $C_p = 0.466\left(\frac{J}{°C.g}\right)$. Since the heat transfer coefficient of air is $5 < h < 30$ (W/m^{2}K), h = 30 was used.

For T_0 = 20 °C and a steady state temperature T = 110 °C the calculated power loss, using Eq. 3.7 is: P_{loss} = 86.9 W.

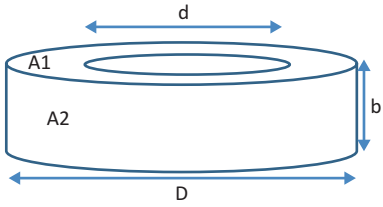

Fig. 3.7 Workpiece thermal contact area

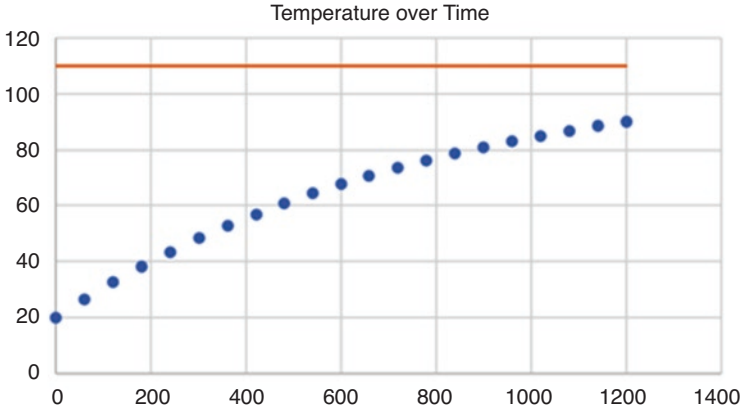

Fig. 3.8 Temperature (°C) over time (seconds) with $P = P_{loss}$

Table 3.1 Heating power for several workpieces

WP	m(Kg)	D(mm)	d(mm)	b(mm)	P(W)	Ptot(W)
1	1,65	140	80	26	311,4	318,0
2	3,40	160	90	40	614,0	623,9
3	3,70	180	100	34	672,0	683,3
4	4,05	170	80	39	730,6	742,3
5	5,15	200	110	38	923,6	937,7
6	6,50	215	120	42	1155,5	1171,8
7	6,80	200	110	53	1201,8	1217,9
8	7,50	220	150	56	1317,4	1333,9
9	8,30	230	130	46	1460,7	1479,4
10	8,45	190	90	64	1473,9	1491,0
11	8,50	310	200	34	1538,2	1563,4
12	10,7	280	200	60	1879,3	1902,8
13	11,3	320	240	60	2000,8	2028,0
14	12,5	215	100	73	2158,6	2180,7

There is also power dissipated by radiation:

$$P_{rad} = \sigma \varepsilon A T^4. \tag{3.9}$$

In Eq. 3.9, σ is the Stefan–Boltzmann constant, ε is the workpiece emissivity, A is the radiant surface and T its temperature in Kelvin. For the given data, and using Eq. 3.9, the power dissipated by radiation is $P_{rad} = 5,67 \times 10^{-8} \times 0,17 \times 0,0322 \times (110 + 273,15)^4 = 6,7$ W.

Total power losses are $P_{loss} + P_{rad} = 86.9 + 6.7 = 93.6$ W. However, to reach a temperature of 110 °C in 20 min, as recommended, the system must provide 318 W (see Table 3.1), instead of 93.6 W.

In the system under study, the user selects from a list stored in software the family to which the bearing belongs to. Each bearing family is associated with its mass m and some relevant dimensions, allowing to calculate, in runtime, the thyristors firing angle Ψ, to obtain the electrical power required for the correct heating. In Table 3.1, there are some characteristics such as inner diameter, outer diameter and the mass of some selected steel bearings from the SKF manufacturer (SKF, 2022).

The values of the electric power necessary to rise temperature from $T_0 = 20$ °C to $T = 110$ °C in 20 min, were calculated using Eq. 3.8 rewritten as

$$P = \frac{hA\left(T - T_0\right)}{\left(1 - e^{-\frac{hA}{mC_p}t}\right)} \tag{3.10}$$

In Eq. 3.10, it was used for the specific heat capacity of steel $C_p = 0.466\left(\frac{J}{°C.g}\right)$, for the heat transfer coefficient of air h = 30 W/m²K and for the heating time t = 1200 s. In the right column of Table 3.1, it was added the power lost by radiation calculated using Eq. 3.9.

Figure 3.9 shows the temperature evolution over time for workpieces nr.1, nr.7 and nr.14, when supplying the calculated power shown in Table 3.1, using Eq. 3.10, to rise the temperature from $T_0 = 20$ °C to $T = 110$ °C in 20 min. These three pieces were chosen because they correspond to the minimum, intermediate and maximum values of electrical power to be supplied. The temperature profile is the similar for all other workpieces.

With the proposed 3.6 KVA system, we are left with the possibility of using it in a wide range of bearings.

Eddy currents are induced and circulates essentially on the inner surface of the ring closest to the core, since that is where the magnetic field is stronger, and it is

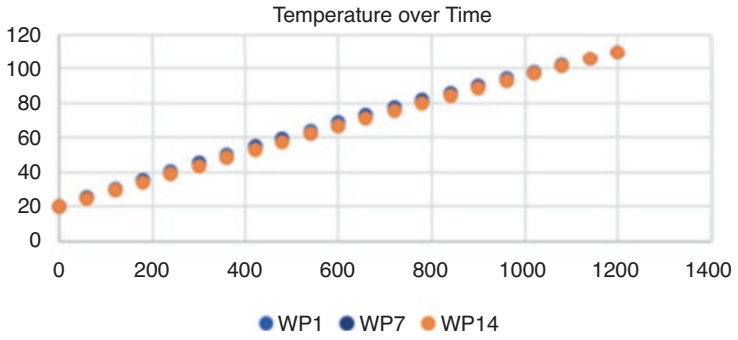

Fig. 3.9 Temperature (°C) over time (seconds) for WP1, WP7 and WP14

also on this surface that the skin effect occurs. The penetration depth of the eddy current comes (Rudnev et al., 2017):

$$\delta_{(T)} = \sqrt{\frac{\rho_{(T)}}{\pi . f . \mu_r \mu_0}} \tag{3.11}$$

The thermal power generated in the workpiece due the Eddy currents can be calculated by the formula (Perrot, 2010):

$$P_o = \frac{\rho}{b} \frac{d}{2\delta} \pi I_w^2 \tag{3.12}$$

where I_w is the induced current in the workpiece, d is the inner bearing diameter and b is its width.

Using Eq. 3.11 on Eq. 3.12:

$$P_o = \frac{\rho}{2b} \frac{d}{\sqrt{\frac{\rho_{(T)}}{\pi . f . \mu_r \mu_0}}} \pi I_w^2 \tag{3.13}$$

The effective eddy current resistance of the workpiece is (from Joule's Law):

$$R_{w(T)} = \frac{\rho}{2b} \frac{d\pi}{\sqrt{\frac{\rho_{(T)}}{\pi . f . \mu_r \mu_0}}} \tag{3.14}$$

where the workpiece electrical resistivity $\rho_{(T)} = \rho_{(20)}[1 + \alpha(T - 20)]$ and α is its the thermal resistivity coefficient. Then

$$R_{w(T)} = \rho_{(20)} \left[1 + \alpha \left(T - 20\right)\right] \frac{d\pi}{2b . \sqrt{\frac{\rho_{(20)} \left[1 + \alpha \left(T - 20\right)\right]}{\pi . f . \mu_r \mu_0}}} \tag{3.15}$$

The current in the workpiece is $I_w = N . I_c$ where $N . I_c$ is the magnetomotive force (mmf) of the system coil. Thus, the equation to calculate the power developed in the workpiece due to the Joule effect comes:

$$P_o = R_{w(T)} . I_w^2 = R_{w(T)} . \frac{N^2}{1} I_c^2 = \left(R_{w(T)} . N^2\right) I_c^2 \tag{3.16}$$

In this system, the coil, the magnetic core and the workpiece behave like a transformer. Therefore, in Eq. 3.16, $R_{w(T)} . N^2$ is the workpiece electric resistance referred to the transformer primary.

It is on this inner surface of the bearing that the temperature rises faster and propagates to the outer ring through the spheres or cylinders. This justifies the need to monitor the temperature difference between the two bearing rings, to avoid structural damage to the spheres/cylinders that would occur due to different thermal dilation of the bearing rings.

3.3.7 Control Algorithm

The proposed algorithm is presented in simplified form in the flowchart of Fig. 3.10. After reading some operator's data, such as the temperature *setpoint*, the maximum temperature difference between the inner and the outer bearing's ring and some other physical bearing characteristics (from bearing family), the initial thyristors firing angle is setup in order to minimize the energy consumption. The *trade-off* power vs heating time is optimized, also ensuring that no structural damage is caused to the bearing, which would occur as result of an excessive temperature difference between its inner and outer rings. The phase load angle is updated at each cycle of the mains. The firing angle is updated at each half cycle of the grid voltage (10 ms, for 50 Hz), using a CPU interrupts routine, so the system's response time is small enough when compared to the thermal time constant of the bearing ($\frac{hA}{mC_p}$ in Eq. 3.8). Such power control method is known as *phase control* (Séguier et al., 2015). In addition, the demagnetization is also assured at the final stage of the heating process, to avoid the aggregation of residues or metallic dust during transportation and placement of the bearing on the machine shaft.

3.4 Experimental Results

All signals are generated in an electronic circuit simulation environment for validation of the proposed control system. Figure 3.11 shows the synchronism pulses generated at zero crossing of the grid voltage (ZCC), the firing pulses for the thyristors T_1 and T_2 with a firing angle $\Psi \approx 95°$ and the voltage at the induction coil.

Figure 3.12 shows the waveforms of the voltage and current in the induction coil for a firing angle $\Psi < \varphi$. As already explained, this is an operating scenario of maximum power at the load but without control. This operation mode, with $\Psi < \phi$, is used at system start up and for a time interval corresponding to only two complete cycles of the grid voltage ($t = 2 \times 20$ ms, for $f = 50$ Hz) to obtain the phase angle φ of the induction coil and thus calculate, at runtime, the minimum possible value to be used for the thyristor firing angle Ψ. However, in some circumstances, it is possible to run the heater at full power with sinusoidal current.

In Figs. 3.13 and 3.14 it is represented, in addition to the firing pulses of the thyristors, the voltage and current in the induction coil for a firing angle $\Psi = 135°$ and $\Psi = 95°$, respectively, showing how current increases for lower firing angles.

In all figures, virtual oscilloscope vertical scales were configured with 20 V/div for load voltage measurements and 0.1 V/div for load current measurements. Current is measured as the voltage drop in a shunt resistor of 0.01 Ohm, resulting in 10 A/div vertical scale. For synchronism pulses, it was selected 1 V/div for vertical scale.

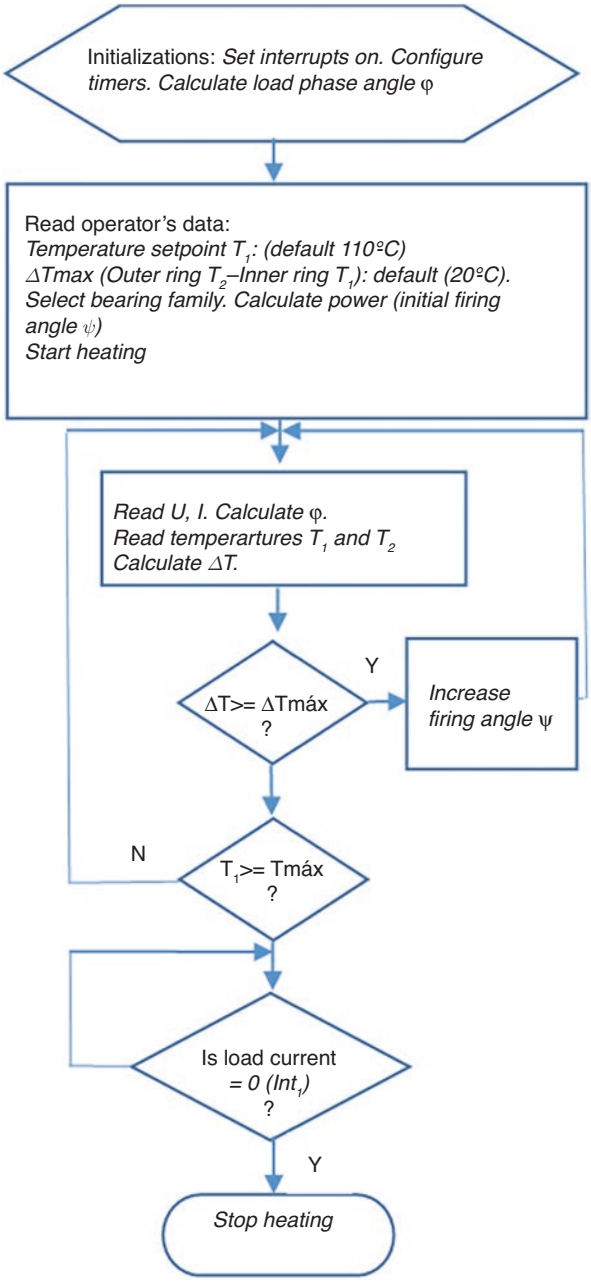

Fig. 3.10 Control algorithm

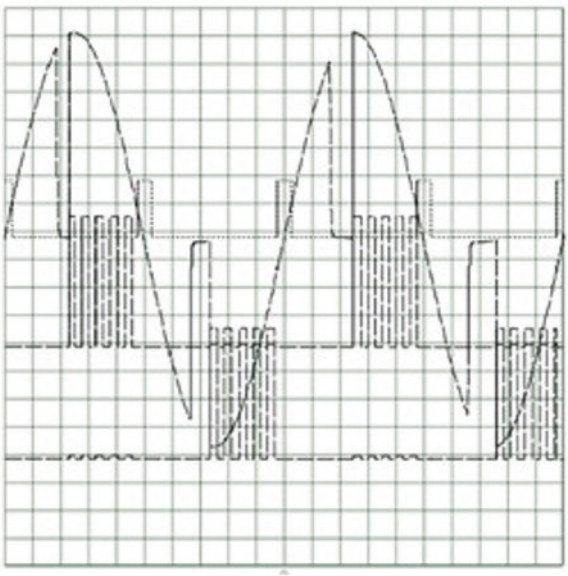

Fig. 3.11 VSync, VtriggerT1, VtriggerT2, V'

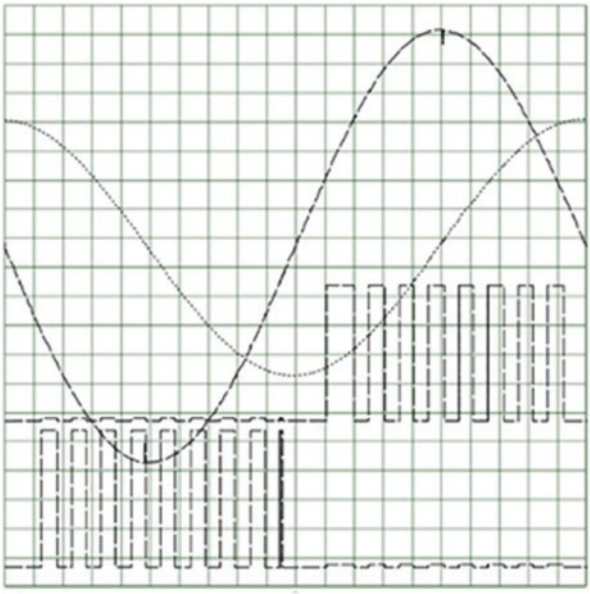

Fig. 3.12 VtriggerT1, VtriggerT2, V' and Io for $\Psi < \phi$. Time base: 1 ms/div

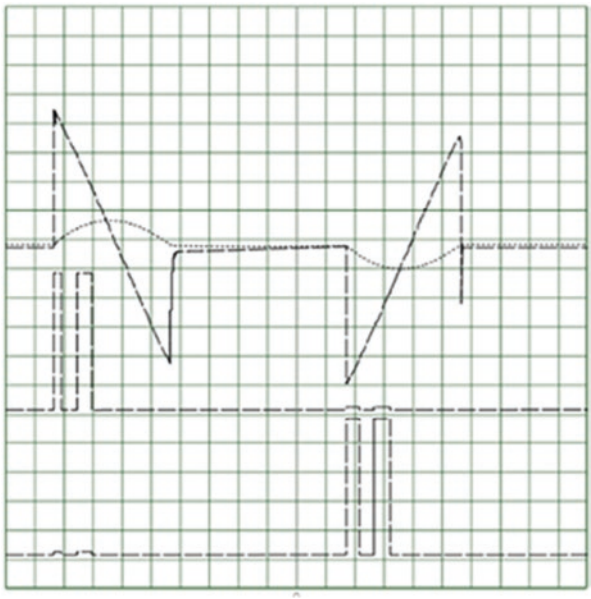

Fig. 3.13 VtriggerT1, VtriggerT2, *V′*, Io, Ψ = 135°. Time base: 2 ms/div

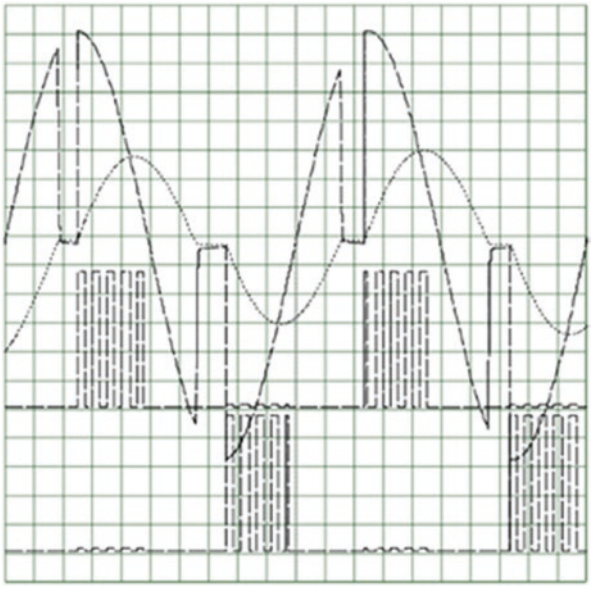

Fig. 3.14 VtriggerT1, VtriggerT2, *V′*, Io, Ψ = 95°. Time base: 1 ms/div

As already stated in Eq. 3.14, the effective Eddy current resistance of the workpiece is

$$R_{w(T)} = \rho_{(T)} \frac{d\pi}{2b.\sqrt{\frac{\rho_{(T)}}{\pi.f.\mu_r\mu_0}}}$$

As the current in the workpiece is $I_w = N.\ I_c$, the power developed in the workpiece due the Joule effect is, according to the Eq. 3.16:

$$P_o = \left(R_{w(T)}.N^2 \right) I_c^2$$

For each workpiece listed in Table 3.2, the coil current needed to develop the required thermal power in the workpiece is

$$I_c = \sqrt{\frac{P_o}{R_{w(T)}.N^2}} \tag{3.17}$$

It was used for the mains frequency $f = 50$ Hz and considered for steel: $\mu_r = 7500$, $\rho_{(20)} = 1.6 \times 10^{-7}\Omega$. m and $\alpha = 6.5 \times 10^{-3}\ K^{-1}$.

In Table 3.2, P_o was calculated using Eq. 3.10, R_w was calculated using Eq. 3.14 and the coil current I_c was calculated using Eq. 3.17.

The payback of a new and more efficient heating system compared to a conventional system can be calculated as follows:

$$\text{Payback}\left(\text{years}\right) = \frac{\text{Investment difference}\left(\text{EUR}\right)}{\text{Annual savings}\left(\text{EUR / year}\right)} \tag{3.18}$$

Table 3.2 Coil current vs. workpiece power

WP	m(Kg)	D(mm)	d(mm)	b(mm)	P_o(W)	$R_w.N^2$(Ω)	I_C(A)
1	1,65	140	80	26	318,0	7,40	6,6
2	3,40	160	90	40	623,9	5,41	10,7
3	3,70	180	100	34	683,3	7,08	9,8
4	4,05	170	80	39	742,3	4,94	12,3
5	5,15	200	110	38	937,7	6,97	11,6
6	6,50	215	120	42	1171,8	6,87	13,1
7	6,80	200	110	53	1217,9	4,99	15,6
8	7,50	220	150	56	1333,9	6,45	14,4
9	8,30	230	130	46	1479,4	6,80	14,7
10	8,45	190	90	64	1491,0	3,38	21,0
11	8,50	310	200	34	1563,4	14,15	10,5
12	10,7	280	200	60	1902,8	8,02	15,4
13	11,3	320	240	60	2028,0	9,62	14,5
14	12,5	215	100	73	2180,7	3,30	25,7

Annual savings in Eq. 3.18 can be calculated using the following formula:

$$\text{Annual savings} = \left(\frac{1}{\eta_{\text{std}}} - \frac{1}{\eta_{\text{new}}} \right) \times Pn \times T \times EC \tag{3.19}$$

where η_{std} and η_{new} are the energy efficiency of conventional heating and induction heating systems, respectively. P_n is the electrical power, in kW, T is the annual operation time, in hours and EC the energy cost in Eur/KWh. The energy efficiency of the heating system is

$$\eta_{\text{new}} = \frac{P_o}{P_o + P_i} \tag{3.20}$$

where P_o is the power in the workpiece and P_i is the power dissipated in the induction coil. According to (Callebaut, 2007), it is expected an energy efficiency in the range between 90% and 97%. The coil power loss P_i is minimized adopting the rules described in the Sect. 3.3, Methodology to build de coil, such as using low resistivity copper, low pitch between turns and a geometric configuration close to that of a solenoid.

As explained before, the thermal power generated in the workpiece by Eddy currents can be calculated by Eq. 3.12: Using Eq. 3.1 in Eq. 3.12: $P_o = \frac{\rho}{b} \pi I_w^2 \frac{d}{2} \sqrt{\frac{\pi . f . \mu_r \mu_0}{\rho}} = \frac{\rho}{b} \pi I_w^2 \frac{d}{2} \sqrt{\frac{\pi . f . \mu_r . 4\pi . 10^{-7}}{\rho}}$

$$P_o = \frac{d}{b} \pi^2 \sqrt{10^{-7} \rho \mu_r f}\, I_w^2 = \frac{d}{b} \pi^2 \sqrt{10^{-7} \rho \mu_r f}\, \left(N . I_c \right)^2 \tag{3.21}$$

where d is the diameter of the inner ring, b is its width, μ_r is the relative magnetic permeability, ρ is the workpiece resistivity (at 110 °C) and f is the frequency of induced current I_w. Equation 3.21 tells that to increase the thermal power in the workpiece, it is better to increase coil current I_c than increasing frequency. In turn, increasing the frequency would increase the reactance of the coil $j\omega L$, which, according to the Ohm's Law, would decrease the current.

To calculate the system's energy efficiency, it is used Eq. 3.20. In that equation, the power loss in the coil is calculated using Joule's Law: $P_i = R_b . I_c^2$, where R_b is the coil electric resistance, and I_c it is the coil current. For the system under study, coil resistance was calculated using Eq. 3.4: $R_b = 7.16$ mΩ.

For workpiece WP1 listed in Table 3.2 ($d = 80$ mm, $b = 26$ mm), P_o is 318 W, $I_c = 6.6$ A and $P_i = R_b . I_c^2 = 0.3$ W. The system's energy efficiency is

$$\eta_{\text{new}} = \frac{318}{318 + 0.3} = 99.9\%$$

For workpiece WP14 listed in Table 3.2 (d = 100 mm, b = 73 mm), P_o is 2180,7 W, I_c = 25.7 A and $P_i = R_b.I_c^2 =$ 4,7 W. The system's energy efficiency is

$$\eta_{\text{new}} = \frac{2180.7}{2180.7 + 4.7} = 99.8\%$$

In the system under study, it was expected to achieve a relevant energy efficiency for the minimum and the maximum electric power, when compared to conventional systems as those described in (SKF, 2022). That being said, there is still the need to verify in the real environment as it was not taken into account the magnetic losses in the system core.

3.5 Conclusions

Induction heating is based on the three following effects: electromagnetic induction, skin effect and heat transfer. Despite the undesirable skin effect in many electrotechnical applications, here, on the contrary, it is used to generate heat with high efficiency (Khatroth et al., 2021; Lucia et al., 2013; Mohan et al., 2003). The increase in electric resistance caused by the workpiece apparent cross section reduction due to skin effect allows getting more thermal power generated by Joule effect.

The proposed solution, it is a system safe and easy to use for its operators, does not pose risks to the environment, ensures low energy consumption to heat steel alloy bearings without compromising their mechanical structural characteristics.

A low frequency such as the utility frequency is used in the proposed system. That is enough for heating a workpiece or even to melt it (Mohan et al., 2003) should that be the case. The phase control used in the AC/AC power converter leads us to have to correct the power factor using an input capacitive filter. This is important to do, especially in low power operating scenario, where the third harmonic amplitude is predominant and the reactive power exceeds the active power (Séguier et al., 2015). In future developments, the focus will be also in high frequency induction heating, using resonant power converters, to achieve a better *power factor* but also to heat materials other than metals (e.g. ceramic workpieces).

The usage of the proposed system is not restricted to the described application. In fact, there is a wide spectrum of applications where energy consumption and user safety are mandatory in heating systems, as in the case of cooking devices (Khatroth et al., 2021) and other household and industrial appliances (Shen et al., 2006; Takau, 2015).

It is also pursued the objective of developing a fully functional prototype of an induction heater to support the training of our students and engineers.

References

Callebaut, J. (2007). Laborelec, «Chauffage par induction». *Leonardo ENERGY. Guide Power Quality* (7). https://www.econologie.com/file/technologie_energie/Chauffage_par_induction.pdf

Khatroth, S., Porpandiselvi, S., & Vishwanathan, N. (2021). Three-load cyclic controlled single-stage AC-AC resonant converter for induction cooking applications. In *2021 IEEE 2nd international conference on Smart Technologies for Power, Energy and Control (STPEC)* (pp. 1–6). IEEE. https://doi.org/10.1109/STPEC52385.2021.9718631

Lucia, O., Maussion, P., Dede, E. J., & Burdío, J. M. (2013). Induction heating technology and its applications: Past developments, current technology, and future challenges. *IEEE Transactions on Industrial Electronics, 61*(5), 2509–2520. https://doi.org/10.1109/TIE.2013.2281162

Microchip. (2022). *Atmega328*. https://www.microchip.com/en-us/product/atmega328p

Mohan, N., Undeland, T. M., & Robbins, W. P. (2003). *Power electronics: Converters, applications, and design*. Wiley.

Perrot, O. (2010). Cours D'Électrothermie. *IUT de Saint-Omer dunkerque département Génie Thermique et l'énergie, (2010–2011)*. https://sitelec.org/download_page.php?filename=cours/electrothermie.pdf

Radvan, L. (2014). *Fast thyristors. When burning for induction heating solutions*. https://search.abb.com/library/Download.aspx?DocumentID=PEE_82014&LanguageCode=en&DocumentPartId=&Action=Launch

Rudnev, V., Loveless, D., & Cook, R. L. (2017). *Handbook of induction heating*. CRC Press. https://doi.org/10.1201/9781315117485

Séguier, G., Delarue, P., & Labrique, F. (2015). *Electronique de puissance* (10e éd.)*: Structures, commandes, applications*. Dunod.

Shen, H., Yao, Z. Q., Shi, Y. J., & Hu, J. (2006). Study on temperature field induced in high frequency induction heating. *Acta Metallurgica Sinica (English Letters), 19*(3), 190–196. https://doi.org/10.1016/S1006-7191(06)60043-4

SKF. (2022). *Aquecedores por indução*. https://www.skf.com/pt/products/maintenance-products/bearing-heaters/heaters-for-mounting/induction-heaters

Takau, L. (2015). Improved modelling of induction and transduction heaters. PhD thesis in Electrical and Computer Engineering at the University of Canterbury. https://doi.org/10.26021/2756

Umans, S. D., Fitzgerald, A. E., & Kingsley, C. (2014). *Máquinas elétricas* (7ªed.). Bookman.

Villate, J. E. (1999). *Eletromagnetismo*. McGraw-Hill.